Lab on a Chip

Accepted Manuscript

ROYAL SOCIETY OF CHEMISTRY

www.rsc.org/loc

Lab on a Chip

RSCPublishing

ARTICLE

Microfluidic Platform Generates Oxygen Landscapes for Localized Hypoxic Activation

Cite this: DOI: 10.1039/x0xx00000x

Megan L. Rexius,[a] Gerardo Mauleon,[a] Asrar B. Malik,[b] Jalees Rehman,[b,c] and David T. Eddington[a*]

Received 16th July 2014,
Accepted 00th January 2014

DOI: 10.1039/x0xx00000x

www.rsc.org/

An open-well microfluidic platform generates an oxygen landscape using gas-perfused networks which diffuse across a membrane. The device enables real-time analysis of cellular and tissue responses to oxygen tension to define how cells adapt to heterogeneous oxygen conditions found in the physiological setting. We demonstrate that localized hypoxic activation of cells elicited specific metabolic and gene responses in human microvascular endothelial cells and bone marrow-derived mesenchymal stem cells. A robust demonstration of the compatibility of the device with standard laboratory techniques demonstrates the wide utility of the method. This platform is ideally suited to study real-time cell responses and cell-cell interactions within physiologically relevant oxygen landscapes.

Introduction

Cells are sensitive to the partial pressure of oxygen, and the precise sensing of distinct oxygen levels triggers potent biological responses. A wide variety of biological processes are impacted by oxygen tension, including embryonic development,[1, 2] stem cell differentiation,[3] metabolism,[4] angiogenesis,[5] and tumorigenesis.[6, 7] Oxygen tension below physiological levels (hypoxia) results in extensive alterations in gene expression. Virtually all hypoxia-related alterations in gene expression rely on the transcriptional activity of the hypoxia inducible factor (HIF) family of transcriptional factors.[8-10] HIF activation is a master switch for a vast array of hypoxia-induced cell signaling pathways. Following exposure to low oxygen levels, HIF α-subunits undergo rapid accumulation, nuclear translocation, heterodimerization with the β-subunit, and binding to initiate transcription of target genes.[11-13]

To study cellular behavior as a result of HIF activation, hypoxia chambers or workstations have been widely used to establish hypoxic environments. Existing hypoxia chambers have the disadvantage of leaving a large footprint, requiring relatively long equilibration times, and providing only a homogenous hypoxic level across a cell culture. The single oxygen level macroenvironments in such culture systems do not provide the oxygen gradients characteristic of the highly heterogeneous oxygen landscapes found at the physiological setting or control at the microscale.[14, 15]

Oxygen gradients occur naturally due to transport limitations of oxygen and the metabolic consumption of oxygen by surrounding cells. Within tissue, different cells are exposed to distinct oxygen levels because the oxygen supply to a given cell is limited by the diffusion distance of the cell from microvessels.[15]

To improve the biological study of hypoxia, microfluidic devices have been developed to permit tight control of oxygen levels exposed to cultured cells and have been used by multiple groups for close monitoring of cell and tissue responses to hypoxia.[16-22] Such devices have often used only single oxygen levels or established multi-condition oxygen levels relying on computer-controlled off-chip gas mixers,[21] flow of media perfusate,[22] flow of oxygen scavenging chemicals,[17, 20] or precise on-chip gas mixer layouts.[19] Although microscopy is performed in these devices, they are not well-suited for other standard cellular, molecular, and biochemical assessments of cell signaling. Designs that culture cells within closed microchannels, as opposed to the open-well format, complicate harvesting the cells for downstream analysis. Another limitation of existing devices is their small size. For example, they do not accommodate enough cellular material for western blot analysis.

To fulfill this unmet need, we have developed a large-area open-well culture platform that maintains a stable oxygen gradient and does not require the incorporation of a gas mixer or a syringe pump for perfusion of liquids. The open-well

design eliminates culturing cells in closed microchannels, accommodates standard biochemical assays, and permits real-time monitoring of interactions between differentially oxygenated cells. By designing different gas networks, we are able to achieve a variety of oxygen landscapes to which cell cultures or tissue slices can be exposed. We have previously shown our methods using gas-perfused networks and diffusion across gas-permeable membranes are successful for controlling oxygen in brain slices[23] and 3D gels.[24] Here we demonstrate designs for binary, square wave, oscillating, and linear gradient oxygen profiles. We focus on utilizing the binary dual condition landscape and further detail the device layout and operation. We characterized the device with oxygen measurements, and then provide a robust demonstration of the utility of the dual condition design in which two different inlet gases are used to impose a steep gradient across a confluent monolayer of cells. Compared to designs that achieve oxygen gradients using on-chip channel mixing for generation of gradient environments,[19] the dual condition oxygen gradient is stable, and the oxygen levels can be reliably determined as a function of position in the device. With an in-channel mixing approach, small fluctuations in pressure of the inlet compressed gases shift the spatial position of the gradient dramatically. In our dual condition design, there are discrete networks for each oxygen condition separated by a diffusion gap between adjacent networks. The gradient is fixed by the architecture and is unaltered by fluctuations in pressure. Here we also demonstrate cell signaling analysis of human cells (both mature endothelial cells and stem cells) in our novel dual condition platform that permits the investigation of real-time responses across a heterogeneous oxygen landscape with a stable oxygen gradient. Our results include immunofluorescent staining of HIF-1α, Western blot detection of a classic HIF-1α target gene in human lung microvascular endothelial cells (HLMVECs), and the relative gene expression of metabolic genes in human bone marrow-derived mesenchymal stem cells (MSCs).

Experimental

Microfluidic device design and fabrication

The polydimethylsiloxane (PDMS) platform (Fig. 1A) was a multilayer construction. Standard SU-8 lithography techniques were used for microfabrication wherein channel features were replicated in PDMS (Sylgard 184 Silicone Elastomer; Dow Corning Corp., Midland, MI) from SU-8 masters. PDMS was chosen for its well-characterized oxygen diffusivity, biocompatibility, and optical clarity. First, a PDMS channel network layer (cured at 85°C on a hot plate for 2 hr) was punched with inlet/outlet ports (3.2 mm diameter). Second, the thin, PDMS membrane was made by spinning uncured, degassed PDMS on a 100 mm diameter silicon wafer (Silicon Sense, Inc., Nashua, NH) at 800 rpm for 30 s using a spin coater (Laurell Technologies Corporation, North Wales, PA). After curing at 60°C for 50 min, the 100 µm-thick membrane was bonded to the channel network layer using a 3 min surface treatment from a handheld corona discharge device (Electro Technic Products, Chicago, IL). The corona discharge device was used in room air at room temperature at its maximum output power of 30 watts. The bonded membrane was punched with inlet/outlet ports, and the PDMS construct was then bonded on a 75 mm x 50 mm glass slide (Fisher Scientific). The open-well spacer layer was cut as a rectangle of PDMS (8 mm thick) with outer dimensions equal to those of the channel network construct with matching access ports. An inner rectangle of PDMS (offset 9.35 mm from the shorter of the rectangular edges and 11.6 mm from the longer edge) was removed to create the walls of the open well. The open-well spacer layer was punched with matching access ports and bonded on top of the PDMS membrane.

A variety of oxygen landscapes were realized using our design and fabrication methods (refer to supplement Fig. S1A - Fig. S1D). We show our design for binary, square wave, oscillating, and linear gradient oxygen profiles. All the profiles were able to be achieved with only two different gas compositions (0% O_2 and 21% O_2) with the exception of the linear gradient (see the supplement for further details). Of these different landscapes, we focus on the dual condition binary landscape (Fig. S1A) created with two microfluidic perfusion networks (500 µm wide and 300 µm deep) separated by a 500 µm wide gap. A gas composition of 5% CO_2, balanced nitrogen flowed through the left network and 5% CO_2, balanced air flowed through the right network (Fig. 2A). The device dimensions gave a ≈14 cm^2 cell culture area which was approximately 1.5 times the area of a well in a standard 6-well plate. Using the binary dual condition design with hypoxic oxygen levels flowing through one network and normoxic oxygen levels flowing through the adjacent network, distinct regions of differential oxygenation and a steep gradient in the diffusion gap were imposed on a cell monolayer (Fig. 2B).

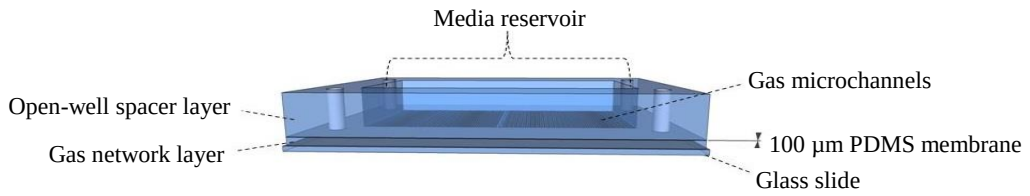

FIGURE 1. The open-well microfluidic platform generates oxygen landscapes across a cell culture. The multi-layered construction consists of a glass slide, gas network layer with microchannels, 100 µm thick PDMS diffusion membrane, and open-well spacer layer which forms the media reservoir.

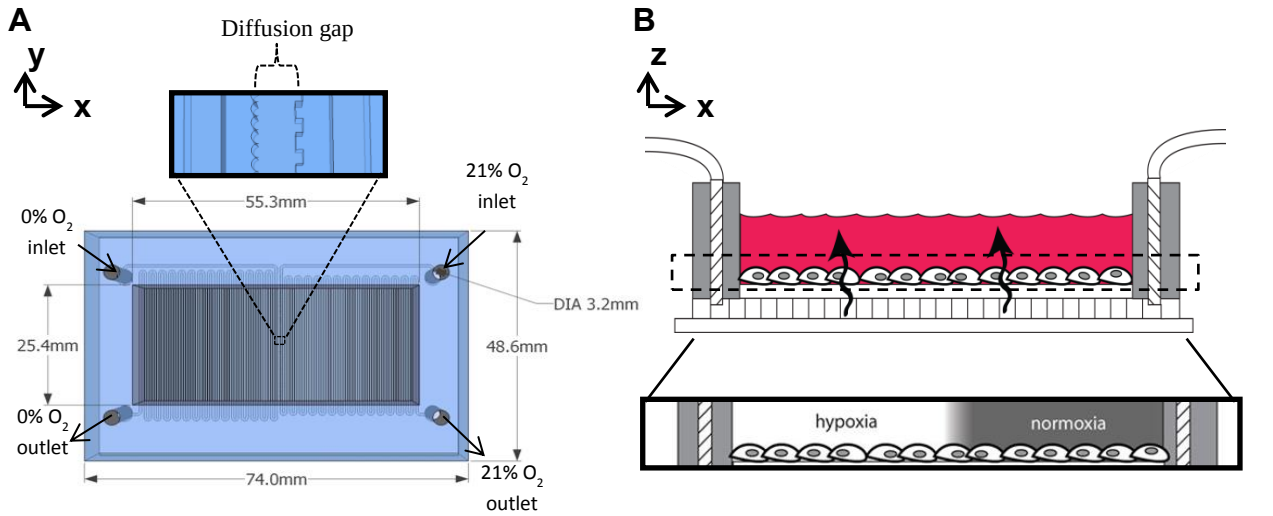

FIGURE 2. Device schematic of the open-well microfluidic platform for generating oxygen landscapes across a cell culture. (A) Dimensions detail the device layout and provide a large culture area. Adjacent serpentine networks are separated by a 500 µm diffusion gap designed with edge microfeatures for easy identification under a microscope. (B) The cross-sectional schematic demonstrates how the device functions. The choice of inlet gases permits a dual condition oxygen landscape to be established close to the membrane with a steady hypoxic region (white), a steady normoxic region (grey), and a steep gradient in the diffusion gap.

Oxygen profile validation

The surface oxygen profile was characterized using a polystyrene and platinum(II) octaethylporphyrinketone (PtOEPK) thin film in contact with the 100 µm PDMS membrane. The fluorescence of the PtEOPK fluorophore in the film is quenched in the presence of oxygen, and its fabrication is described elsewhere.[25] Briefly, polystyrene was dissolved in toluene (35% w/w toluene/PS), then 0.5 mg mL^{-1} of PtOEPK was added to the toluene/PS mixture.

With the sensor on top of the PDMS membrane, the device was filled with 5 mL of water prior to beginning gas perfusion. Scanning imaging was used to determine the surface percent oxygen profile. Scans were taken 1 hr after introducing gas flow. Fluorescent intensity in the images was converted to percent oxygen by solving the Stern-Volmer equation.[26] Scans of the sensor in 5% CO_2, balanced nitrogen and 5% CO_2, balanced air were used to calibrate the sensor measurements.

The dissolved oxygen content was measured using a hand-held optical sensor (Neofox; Ocean Optics). The tip of the oxygen probe contains a ruthenium compound that is quenched in the presence of oxygen. Sensor calibration was performed according to the manufacturer's instructions. During calibration, first 5% CO_2, balanced nitrogen was injected into both microfluidic networks, and then only 5% CO_2, balanced air was injected through the device. An electronic manipulator was used to hold the oxygen probe and adjust the x, y, and z planes with a resolution of 0.1 µm inside the open well. We used the electronic manipulator to precisely adjust the vertical distance of the probe's tip from the surface of the PDMS membrane within the well.

Oxygen modulation was performed by constant perfusion of desired gas compositions from compressed gas tanks. Plastic connectors (McMaster-Carr) were inserted into the cored access ports of the device. Tygon tubing with a 1/16 inch inner diameter and 1/8 inch outer diameter (Cole-Parmer, Vernon Hills, IL) interfaced with the device, and a glass tube rotameter (Omega Engineering, Inc., Stamford, CT) was used to control the gas flow rate. Gases were flowed at a rate of 30 mL/min through the device.

Cell culture

Fabricated devices were autoclaved at 121°C for 30 min prior to use. Then, 2 mL of 0.1% gelatin (porcine skin type A; Sigma-Aldrich) in E-pure water (Barnstead Thermolyne, Dubuque, IA) was added to the open-well reservoir and incubated at 37°C overnight. After excess gelatin was aspirated, cells were seeded at 300,000 cells per device in 5 mL of the associated culture media. HLMVECs (HMVEC-L; Lonza) were cultured in EGM-2 with supplements (EGM-2 MV with bullet kit; Lonza). Human bone marrow-derived MSCs (hMSC; Lonza) were cultured in complete culture medium (CCM) with fetal bovine serum (FBS), which is comprised of Minimum Essential Medium Alpha (αMEM), 20% FBS, 2 mM L-glutamine, and 100 units/mL penicillin and streptomycin. Devices seeded with cells were placed in petri dishes and housed in a standard incubator at 37°C in 5% CO_2, balanced air. Prior to oxygen modulation studies, media was changed every 24 hr until cells reached >90% confluency.

In-device immunofluorescent staining

Immunofluorescent staining of transcription factor HIF-1α was performed on a confluent monolayer of HLMVECs after 12 hr of dual condition constant perfusion. Cell culture media was carefully aspirated, and the cells were then washed three times with 4°C PBS, fixed with 4% paraformaldehyde for 10 min at room temperature, and washed three additional times with PBS. Cells were permeabilized in 0.2% Triton X-100 in PBS for 10 min at room temperature, washed three times with PBS, and blocked in blocking buffer (X0909; Dako, Carpinteria, CA) for

1 hr at room temperature. Cells were subsequently incubated with anti-HIF-1α antibody (Novus Biologicals, Littleton, CO) with a 1:100 dilution in antibody diluent (S3022; Dako) in a humidified chamber overnight at 4°C. After three washes with Tris-buffered saline with Tween-20 (TBST; Boston Bioproducts, Boston, MA), cells were incubated with fluorescent secondary antibody (Alexa Fluor 488; Invitrogen, Carlsbad, CA) in antibody diluent with a 1:300 dilution for 2 hr at room temperature. Cells were washed three times with TBST and nuclei were stained (Hoechst 33342; Invitrogen) with a 1:5000 dilution in washing buffer (10 mM Tris HCl, pH 7.4, 100 mM NaCl, and 0.10% Tween-20 in distilled water) for 20 min at room temperature.

Protein extractions and western blotting

With the injected gases still flowing through the device, the device was placed on ice. Media was aspirated, and the cells were washed twice with cold phosphate buffered saline (PBS) containing 10 mM phenylmethylsulfonyl fluoride (PMSF). A volume of 100 µL PBS was added back to the well and cells were separately scraped from the leftmost third of the device (a 25.4 mm by 18.4 mm area) and the rightmost third of the device with a cell scraper. In the dual condition configuration, the leftmost third corresponded to a region of steady hypoxia and the rightmost third corresponded to a region of steady normoxia. Cells cultured on the central third of the device's membrane, containing the gradient region of the dual condition configuration, were also collected for analysis (data not shown). Then, the cells from each of these regions were collected in a separate pipet tip and transferred to a microcentrifuge tube. The cells were centrifuged at 1400 rpm for 5 min at a temperature of 4°C. The remaining PBS was aspirated from the cell pellet, and the pellet was resuspended in 50 µL of RIPA buffer (10 mM Tris [pH 8.0], 140 mM NaCl, 1% Triton X-100, 1% sodium deoxycholate, and 0.1% sodium dodecyl sulfate [SDS]) for total cell lysis. Lysates were incubated on ice for 15 min with intermittent vortexing. Protein concentration of each lysate was determined by the BCA assay (Pierce BCA Protein Assay Kit; Thermo Scientific) using bovine serum albumin as the protein concentration standard.

Equivalent amounts of protein (30 µg) were separated by SDS-PAGE and then transferred to nitrocellulose membranes using standard procedures. The membrane was blocked with 3% bovine serum albumin (BSA) in Tris-buffered saline (TBS) for 1 hr. After blocking, membranes were incubated at 4°C overnight with 3% BSA in TBS, containing anti-LDHA (Santa Cruz Biotechnology, Dallas, TX). After 3 washes in TBS with 0.05% Tween (TBST), membranes were incubated with corresponding horseradish peroxidase-conjugated secondary antibodies in 5% milk in TBST (1:5000) for 1 hr. A final series of three washes (10 min each) in TBST were performed before developing the blots according to kit directions (SuperSignal West Pico Chemiluminescent Substrate; Thermo Scientific).

Quantitative real-time PCR

After 24 hr of dual condition constant perfusion, relative gene expression of Glut1, PDK isozymes, and LDHA in human MSCs was determined using quantitative real-time PCR. First, media was aspirated and cells were washed three times with room temperature PBS. The device was cut in equal thirds (a left, middle, and right section) to ensure separation of the cells subjected to distinct oxygen levels. The cells were then scraped off each section with a cell scraper and lysed in 300 µL of lysis buffer. Lysis buffer consisted of 10 µL of β-mercaptoethanol (Sigma Aldrich) per 1 mL of lysis buffer (PureLink RNA Mini Kit; Invitrogen). The lysates were collected in a pipet tip and transferred to an RNAse/DNAse-free microcentrifuge tube and placed in -80°C for storage prior to RNA isolation. RNA was extracted with a PureLink RNA Mini Kit (Invitrogen) according to the manufacturer's instructions.

Synthesis of cDNA from total RNA was performed using a High-Capacity cDNA Reverse Transcription Kit (Applied Biosystems, Foster City, CA), and RT-PCR was carried out on Applied Biosystems ABI PRISM 7000 detection system in 25 µl reactions containing 12.5 µl of TaqMan Gene Expression Master Mix. Relative gene expression of target gene mRNA was performed using TaqMan Gene Expression Assays (Applied Biosystems) and was calculated using beta-2-microglobulin (B2M) as the endogenous control.

Statistical analysis

All human cell culture experiments were repeated at least three independent times, and data are expressed as the mean ± SEM. Significance was determined from one-way ANOVA with Tukey's multiple comparison post-test. Analyses were performed with Prism 5 by Graphpad.

Results and discussion

Dual condition oxygen landscape

The device was used in three configurations: (1) hypoxia (both channel networks 95%N_2/5%CO_2), (2) normoxia (both channel networks air/5%CO_2), or (3) dual condition (one network 95%N_2/5%CO_2, one network air/5%CO_2). A fluorescent PtOEPK thin film sensor placed on top of the PDMS membrane characterized the oxygen profiles (Fig. 3A). The surface percent oxygen was calculated from fluorescent intensities by solving the Stern-Volmer equation. Results were plotted as a function of position in the x-direction (Fig. 3B). The slope of the oxygen gradient between the two adjacent microfluidic networks was 11.4 %/mm, which equates to a 1% change in oxygen tension every 87.7 µm. We measured the dynamics of inducing hypoxic conditions in the device and plotted the percent oxygen at the surface of the membrane as a function of time (Fig. 3C). Our experimental data demonstrated that the time required to achieve steady-state diffusion of oxygen across a 100 µm PDMS membrane was approximately 20 seconds.

Constant perfusion of 95%N_2/5%CO_2 in the underlying microfluidic channels maintains severe hypoxic conditions for cells in the hypoxic region of the device when operated in the

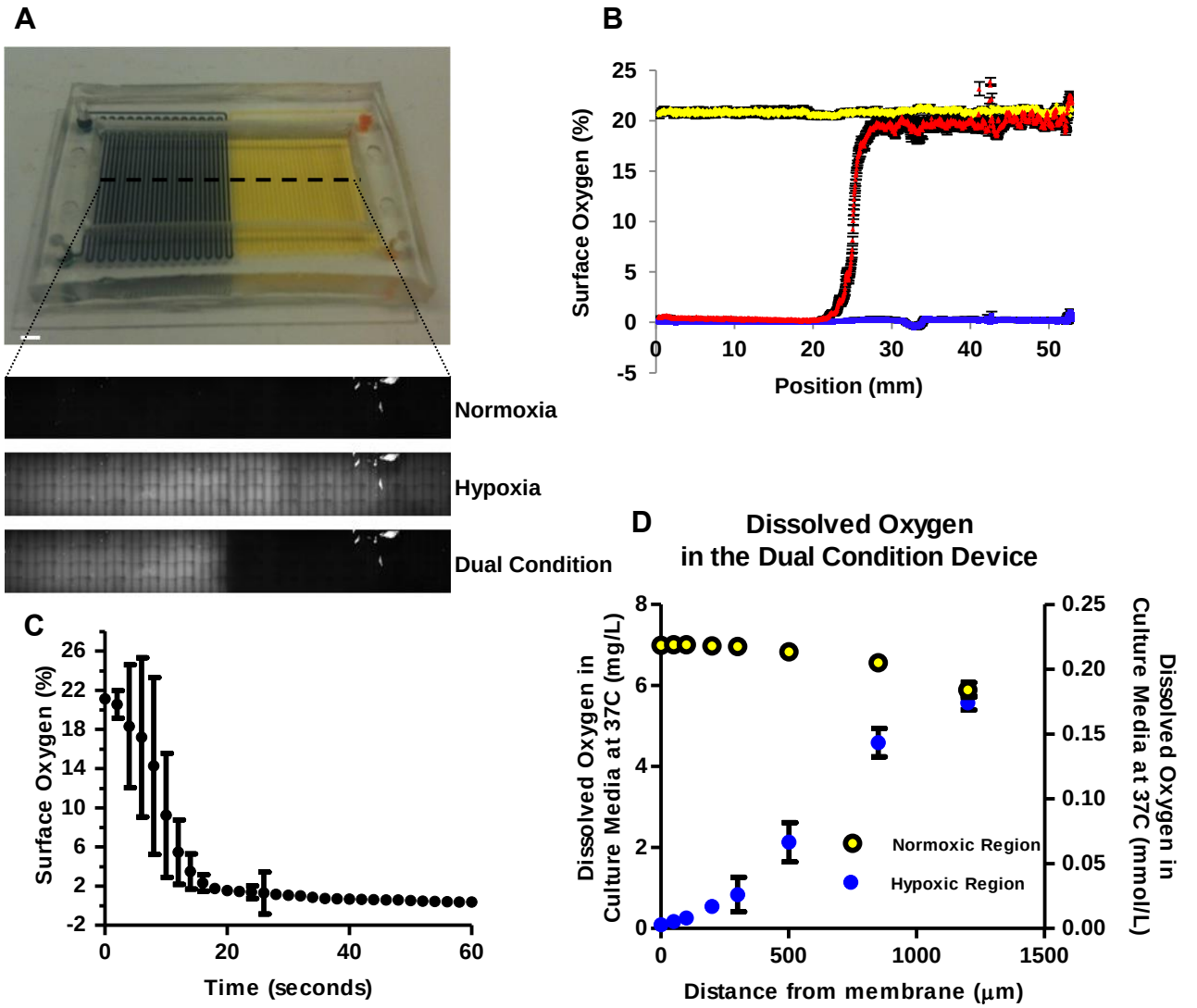

FIGURE 3. Sensor measurements characterized the dual condition oxygen profile. (A) Two dyes (blue and yellow) injected into the adjacent serpentine microchannel networks clearly delineate the boundaries. Scale bar, 4 mm. Fluorescent image scans were performed across the width of the culture space in three configurations: normoxia, hypoxia, and dual condition. The fluorophore within the sensor, platinum(II) octaethylporphyrinketone (PtOEPK), is quenched in the presence of oxygen. (B) The surface percent oxygen is shown as a function of position with plots of normoxia (yellow), hypoxia (blue), and the dual condition (red) configuration (mean ± SEM, n=3). (C) The surface oxygen percent as a function of time demonstrates the rapid equilibrium of hypoxic induction in the device (mean ± SD, n=3). (D) In the open-well format, the concentration of dissolved oxygen equilibrates as the distance from the PDMS membrane increases due to exchange with the controlled 5% CO2, balanced air and 37ºC conditions inside the cell culture incubator (mean ± SD, n=3).

dual condition configuration and severe hypoxic conditions for the entire monolayer of cells when operated in the homogenous hypoxia configuration. The dual condition configuration maintained inlet gas oxygen levels within 100 μm of the membrane, making it ideally suited for studying cells or thin tissue slices (Fig. 3D). In hypoxia, we show that the dissolved oxygen increases rapidly as the distance from the membrane increases. This is caused by the gas exchange that occurs with the surrounding controlled gas conditions in the incubator (5% CO_2, balanced air at 37°C). While our oxygen measurements do not give us the resolution to precisely determine the hypoxic conditions experienced by the cells on the membrane, we estimate that they are ≤ 0.5% oxygen. The device was used to look at a binary profile from 0% to 21% oxygen, but any binary condition could be studied by injecting different gases into the networks.

Hypoxic response of human microvascular endothelial cells

We first tested the biological responsiveness of human cells in the platform. Hypoxia-induced alterations in gene expression rely on the transcriptional activity of the HIF family of transcriptional factors.[27] Following low oxygen levels, HIF-α-subunits (HIF-1α, HIF-2α, and HIF-3α) undergo nuclear translocation, heterodimerization with the β-subunit, and DNA binding to initiate transcription of target genes.[5, 8] Human lung microvascular endothelial cells (HLMVECs) cultured in the platform confirmed nuclear translocation of HIF-1α in the

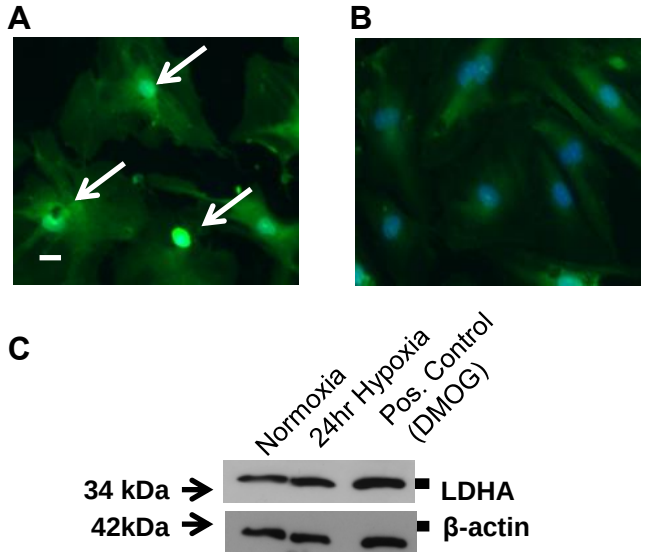

FIGURE 4. Cells respond to oxygen modulation in the platform. (A-B) In-device immunofluorescent staining shows HLMVECs after 12 hr of oxygen modulation. HLMVECs were stained for HIF-1α (green), and nuclei (blue) were counterstained with Hoechst. Punctuated green nuclear staining (indicated by white arrows) shows translocation of HIF-1α to the nucleus in hypoxia (A) as compared to normoxia (B). Scale bar, 1 μm. (C) A representative Western blot demonstrates LDHA protein level in HLMVECS increased after 24 hr of hypoxia in the device compared to the normoxic control device. DMOG, a PHD inhibitor, served as a positive control. Beta-actin is shown as the loading control.

hypoxic region (Fig. 4A) as compared to the normoxic region (Fig. 4B). HLMVECs fixed in the device and stained for HIF-1α after 12 hr of hypoxic oxygen modulation had punctuated green fluorescent staining in the nuclei. As expected, HIF-1α activation in the device increased protein expression of a downstream target gene, lactate dehydrogenase A (LDHA) after 24 hr of oxygen modulation (Fig. 4C). Dimethyloxalylglycine (DMOG) was used as a positive control for HIF activation because it is a prolyl hydroxylase domain (PHD) enzyme inhibitor. Hydroxylation of HIF-1α by a PHD will target the subunit for proteasomal degradation. Therefore, inhibition of PHDs stabilized HIF-1α protein.[28] The protein β-actin served as the loading control.

Metabolic specificity of human bone marrow-derived mesenchymal stem cells

After verifying HIF-1α induction in mature endothelial cells, we studied stem cell function in the oxygen landscape. Human mesenchymal stem cells (MSCs) in vivo are located in the heterogeneous oxygen microenvironment of the bone marrow (BM) to support hematopoietic stem cells (HSCs) by secreting factors for their maintenance.[29] However, it is not understood if an oxygen landscape confers metabolic specificity underlying the dynamic interplay between MSCs and HSCs in the heterogeneous BM microenvironment. The glucose transporter Glut1, LDHA, and four known isozymes of pyruvate dehydrogenase kinase (PDK1, PDK2, PDK3, and PDK4) are genes downstream of HIF-1α that convert metabolic processes from oxidative phosphorylation to glycolysis under hypoxic conditions. Quantitative PCR in MSCs was used to investigate metabolic programs regulated by the oxygen landscape. Homogeneous hypoxia and dual condition hypoxia corresponded with upregulation of the relative gene expression of LDHA (Fig. 5A), indicating an enhanced glycolytic metabolic state during hypoxia compared to normoxia (Fig. 5B). Relative expression of Glut1, PDK1, and PDK3 were also upregulated in homogenous hypoxia and dual condition hypoxia (Fig. 5C). PDK3 expression was more sensitive to the landscape than PDK1, and relative expression of PDK4 was too low for analysis (data not shown). The relative gene expression of PDK2 was insensitive to oxygen tension. Increased gene expression in hypoxia has been reported for PDK4 but not for PDK2 in long-term HSCs (LT-HSCs).[4] Our results indicate not only differential regulation of PDKs dependent on oxygen tension in MSCs but also regulation of regional metabolic profiles in cells by the oxygen landscape itself.

Conclusions

In summary, the results demonstrate analysis of cell responses in an oxygen landscape. The advantage of having cells with different states of HIF activation in the same open well is that it allows assessment of how the cells interact across the oxygen gradient. Our tool presents an opportunity to fundamentally advance hypoxia research because current homogenous oxygen systems do not allow crosstalk between cells exposed to different oxygen levels. The design lends itself to future study of the crosstalk interactions of differentially oxygenated cells with respect to cell-cell contact (because there is a single confluent monolayer of cells) and secreted factors (because there is a single, shared reservoir of culture medium). Real-time PCR results of the relative gene expression of LDHA, Glut1, PDK1, and PDK3 demonstrated that the spatial layout of the oxygen landscape can be resolved in the expression of genes that are under the transcriptional activity of HIF-1α. By examining metabolic genes in MSCs, we showed for the first time the metabolic profile of hypoxic cells in an oxygen landscape with normoxic neighbors is similar to that of cells in homogenous hypoxia. However, in addition to regulating MSC metabolism, hypoxia is a central regulator of paracrine signals involved in stem cell maintenance and cancer progression.[30, 31] The hypoxia-induced secretion of molecules and microvesicles are believed to be the primary source of effects reported in hypoxia-conditioned media experiments. Traditional hypoxia-conditioned medium experiments have the disadvantage of having culture media transferred to other cells at a single, selected time point. Using the dual condition oxygen landscape device, normoxic cells can be exposed to factors from hypoxia-conditioned medium in a real-time and continuous fashion, thereby overcoming the rapid degradation and short half-lives of the secreted molecules present in traditional conditioned medium experiments. Therefore, our new platform is ideal for investigations of real-time, hypoxia-induced effects of the MSC secretome on a differentially oxygenated coculture and lays the framework to address important developmental, regenerative, and pathophysiological responses to oxygen landscapes.

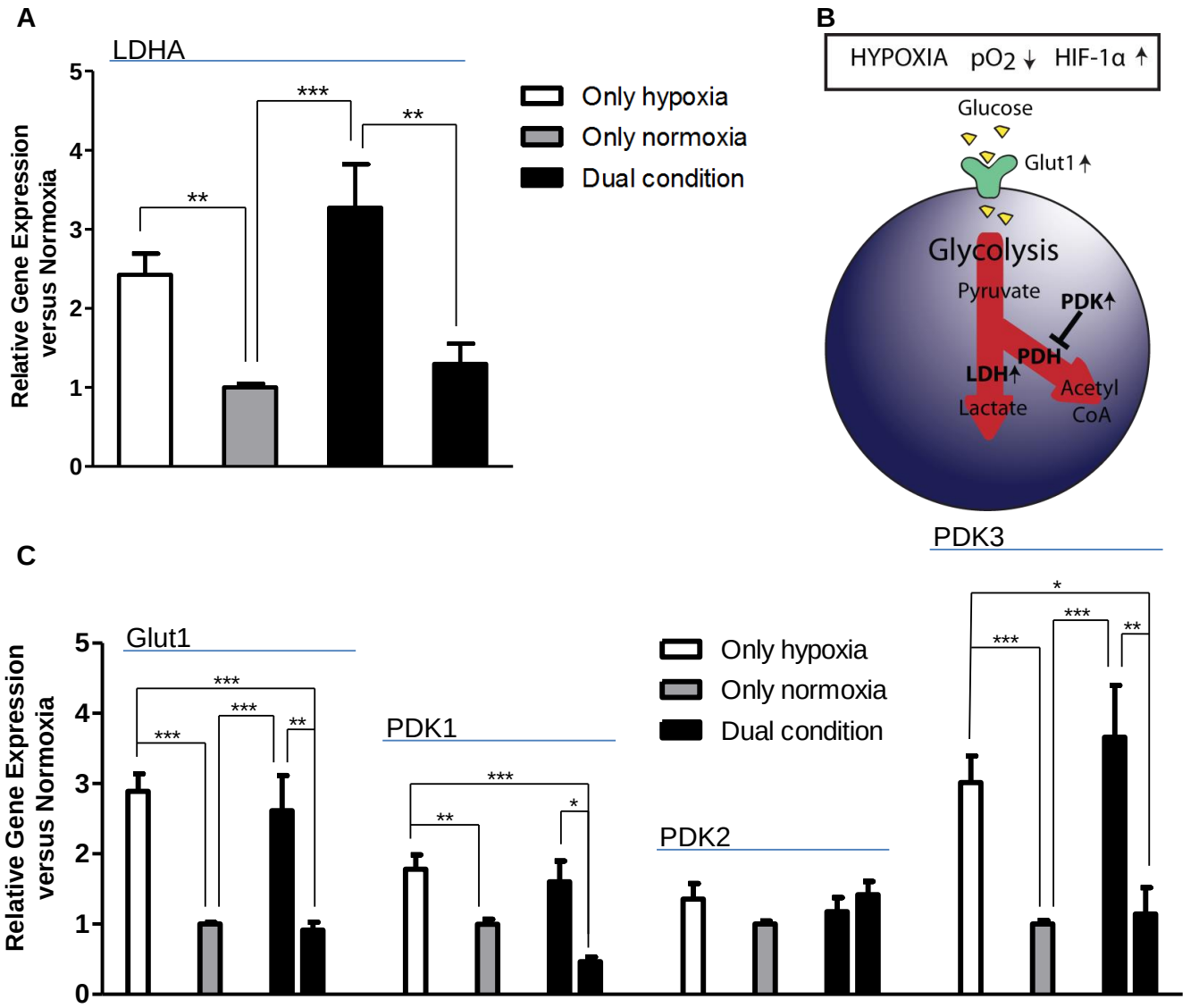

FIGURE 5. The oxygen landscape regulates regional metabolic profiles in bone marrow-derived human mesenchymal stem cells. (A) Quantitative PCR indicates LDHA gene expression is upregulated in the hypoxic region of the oxygen landscape (black, left) as compared to the normoxic region (black, right) and retains the metabolic character of homogenous hypoxic controls (white). (B) The schematic represents the effect of hypoxia on energy metabolism in a cell. (C) Gene expression of Glut1 and the PDK isozymes in homogenous control devices are compared to the dual condition landscape with the hypoxic region (black, left) and normoxic region (black, right). Statistical comparisons were performed with ANOVA and Tukey's multiple comparison post-test (mean ± SEM, n=4, * $p < 0.05$, ** $p < 0.01$, and *** $p < 0.001$).

Acknowledgements

This work was supported by NSF 1253060, NIH T32 HL007829, NIH NCATS UL1TR000050, NIH-R01-GM094220 and the Chicago Biomedical Consortium with support from the Searle Funds at The Chicago Community Trust.

Notes and references

[a] Department of Bioengineering, University of Illinois at Chicago, Chicago, IL 60607, USA. Fax: +1 312 996 5921; Tel: +1 312 355 3278; E-mail: dte@uic.edu

[b] Department of Pharmacology, University of Illinois at Chicago, Chicago, IL 60612, USA.

[c] Section of Cardiology, University of Illinois at Chicago, Chicago, IL 60612, USA.

References

1. S. Dunwoodie, *Developmental cell*, 2009, **17**, 755-773.
2. M. Simon and B. Keith, *Nature reviews. Molecular cell biology*, 2008, **9**, 285-296.
3. A. Mohyeldin, T. Garzón-Muvdi and A. Quiñones-Hinojosa, *Cell stem cell*, 2010, **7**, 150-161.
4. K. Takubo, G. Nagamatsu, C. Kobayashi, A. Nakamura-Ishizu, H. Kobayashi, E. Ikeda, N. Goda, Y. Rahimi, R. Johnson, T. Soga, A. Hirao, M. Suematsu and T. Suda, *Cell stem cell*, 2013, **12**, 49-61.
5. S. Rey and G. Semenza, *Cardiovascular research*, 2010, **86**, 236-242.
6. P. Ratcliffe, *The Journal of physiology*, 2013, **591**, 2027-2042.
7. B. Philip, K. Ito, R. Moreno-Sánchez and S. Ralph, *Carcinogenesis*, 2013.

8. Q. Ke and M. Costa, *Molecular pharmacology*, 2006, **70**, 1469-1480.
9. G. Semenza, *Annual review of cell and developmental biology*, 1999, **15**, 551-578.
10. G. Semenza, *Biochemical pharmacology*, 2002, **64**, 993-998.
11. E. Metzen and P. Ratcliffe, *Biological chemistry*, 2004, **385**, 223-230.
12. R. Chowdhury, A. Hardy and C. Schofield, *Chemical Society reviews*, 2008, **37**, 1308-1319.
13. C. Pugh and P. Ratcliffe, *Nature medicine*, 2003, **9**, 677-684.
14. K. Parmar, P. Mauch, J.-A. Vergilio, R. Sackstein and J. Down, *Proceedings of the National Academy of Sciences of the United States of America*, 2007, **104**, 5431-5436.
15. A. Tsai, B. Friesenecker, M. Mazzoni, H. Kerger, D. Buerk, P. Johnson and M. Intaglietta, *Proceedings of the National Academy of Sciences of the United States of America*, 1998, **95**, 6590-6595.
16. S. Oppegard, K.-H. Nam, J. Carr, S. Skaalure and D. Eddington, *PloS one*, 2009, **4**.
17. Y.-A. Chen, A. King, H.-C. Shih, C.-C. Peng, C.-Y. Wu, W.-H. Liao and Y.-C. Tung, *Lab on a chip*, 2011, **11**, 3626-3633.
18. M. Polinkovsky, E. Gutierrez, A. Levchenko and A. Groisman, *Lab Chip*, 2009, **9**, 1073-1084.
19. J. Lo, E. Sinkala and D. Eddington, *Lab on a chip*, 2010, **10**, 2394-2401.
20. C.-C. Peng, W.-H. Liao, Y.-H. Chen, C.-Y. Wu and Y.-C. Tung, *Lab on a chip*, 2013, **13**, 3239-3245.
21. M. Adler, M. Polinkovsky, E. Gutierrez and A. Groisman, *Lab on a chip*, 2010, **10**, 388-391.
22. G. Mehta, K. Mehta, D. Sud, J. Song, T. Bersano-Begey, N. Futai, Y. Heo, M.-A. Mycek, J. Linderman and S. Takayama, *Biomedical microdevices*, 2007, **9**, 123-134.
23. G. Mauleon, C. P. Fall and D. T. Eddington, *Plos One*, 2012, **7**.
24. S. C. Oppegard and D. T. Eddington, *Biomed Microdevices*, 2013, **15**, 407-414.
25. E. Sinkala and D. Eddington, *Lab on a chip*, 2010, **10**, 3291-3295.
26. M. G. Samantha, C. Lukas and C. C. Karen, *Sensors*, 2010, **10**.
27. S. Greer, J. Metcalf, Y. Wang and M. Ohh, *The EMBO journal*, 2012, **31**, 2448-2460.
28. T. Eckle, D. Köhler, R. Lehmann, K. El Kasmi and H. Eltzschig, *Circulation*, 2008, **118**, 166-175.
29. S. Méndez-Ferrer, T. Michurina, F. Ferraro, A. Mazloom, B. Macarthur, S. Lira, D. Scadden, A. Ma'ayan, G. Enikolopov and P. Frenette, *Nature*, 2010, **466**, 829-834.
30. C. Scheel, E. N. Eaton, S. H. Li, C. L. Chaffer, F. Reinhardt, K. J. Kah, G. Bell, W. Guo, J. Rubin, A. L. Richardson and R. A. Weinberg, *Cell*, 2011, **145**, 926-940.
31. J. M. Roodhart, L. G. Daenen, E. C. Stigter, H. J. Prins, J. Gerrits, J. M. Houthuijzen, M. G. Gerritsen, H. S. Schipper, M. J. Backer, M. van Amersfoort, J. S. Vermaat, P. Moerer, K. Ishihara, E. Kalkhoven, J. H. Beijnen, P. W. Derksen, R. H. Medema, A. C. Martens, A. B. Brenkman and E. E. Voest, *Cancer Cell*, 2011, **20**, 370-383.